HHS Public Access

Author manuscript

Hepatology. Author manuscript; available in PMC 2021 July 01.

Published in final edited form as:

Hepatology. 2020 July ; 72(1): 140–154. doi:10.1002/hep.30970.

Hyperpolarized Metabolic Imaging Detects Latent Hepatocellular Carcinoma Domains Surviving Locoregional Therapy

Nicholas R. Perkons[1,2], **Ryan M. Kiefer**[1,3], **Michael C. Noji**[1,3], **Mehrdad Pourfathi**[3], **Daniel Ackerman**[1,3], **Sarmad Siddiqui**[3], **David Tischfield**[1,3], **Enri Profka**[1,3], **Omar Johnson**[1,3], **Stephen Pickup**[3], **Anthony Mancuso**[3], **Austin Pantel**[3], **Michelle R. Denburg**[4], **Gregory J. Nadolski**[1,3], **Stephen J. Hunt**[1,3], **Emma E. Furth**[5], **Stephen Kadlecek**[3], **Terence P. F. Gade**[1,3,6,*]

[1]Penn Image-Guided Interventions Laboratory, Hospital of the University of Pennsylvania, Philadelphia, PA 19104

[2]Department of Bioengineering, School of Engineering and Applied Science, University of Pennsylvania, Philadelphia, PA 19104

[3]Department of Radiology, Hospital of the University of Pennsylvania, Philadelphia, PA 19104

[4]Department of Nephrology, Children's Hospital of Philadelphia, Philadelphia, PA 19104

[5]Department of Pathology, Hospital of the University of Pennsylvania, Philadelphia, PA 19104

[6]Department of Cancer Biology, Perelman School of Medicine, University of Pennsylvania, Philadelphia, PA 19104

Abstract

BACKGROUND AND AIMS: Advances in cancer treatment have improved survival; however, local recurrence and metastatic disease—the principal causes of cancer mortality—have limited the ability to achieve durable remissions. Local recurrences arise from latent tumor cells that survive therapy and are often not detectable by conventional clinical imaging techniques. Local recurrence after transarterial embolization (TAE) of hepatocellular carcinoma (HCC) provides a compelling clinical correlate of this phenomenon. In response to TAE-induced ischemia, HCC cells adapt their growth program to effect a latent phenotype that precedes local recurrence.

APPROACH AND RESULTS: In this study, we characterize and leverage the metabolic reprogramming demonstrated by latent HCC cells in response to TAE-induced ischemia to enable their detection *in vivo* using dynamic nuclear polarization (DNP) magnetic resonance spectroscopic imaging (MRSI) of ^{13}carbon-labeled substrates. Under TAE-induced ischemia,

*Corresponding author: Terence P. F. Gade, University of Pennsylvania Perelman School of Medicine, 652 BRB II/III, 421 Curie Boulevard, Philadelphia, PA 19104-6160, Tel: 215-573-9756, Fax: 215-746-5511, gadet@pennmedicine.upenn.edu.

AUTHOR CONTRIBUTIONS

MCN and TPG performed in vitro 2D cell culture experiments. MP, SS, AM, and TPG performed the cell perfusion experiment. TPG, NRP, RMK, MP, SS, EP, and SP performed experiments pertinent to the *in vivo* sections of the described work. TPG, RK, EP, SH performed rat embolizations. NRP, MP, and SK developed the Matlab code used to analyze the *in vivo* data. DT, OJ, and EEF performed histologic staining analyses. TPG provided radiologic interpretations. NRP, AP, MRD performed the statistical analyses presented. DA, GJN, SJH, SK, and TPG drove the scientific direction of the completed work. GJN, SJH, and TPG provided clinical context motivating the completed work. NRP and TPG prepared and edited the manuscript and figures, with assistance provided by all co-authors.

latent HCC cells demonstrate reduced metabolism and develop a dependence on glycolytic flux to lactate. Despite the hypometabolic state of these cells, DNP-MRSI of 1-^{13}C-pyruvate and its downstream metabolites, 1-^{13}C-lactate and 1-^{13}C-alanine, predicted histological viability.

CONCLUSIONS: These studies provide a paradigm for imaging latent, treatment-refractory cancer cells, suggesting that DNP-MRSI provides a technology for this application.

Keywords

locoregional therapy; hepatocellular carcinoma; dynamic nuclear polarization

Advances in our understanding of tumor biology and technology have led to the development of novel targeted and locoregional therapies with improved response rates, transforming the prognoses of certain cancers from terminal into chronic diseases (1). Improved survival has been accompanied by a concomitant increase in the incidence of recurrent local and metastatic disease (2,3). These recurrences are thought to arise from cancer latency wherein remnant or disseminated cancer cells persist without detectable growth (4). Given that the large majority of cancer-related deaths result from metastatic disease, the ability to characterize and ultimately target latent cancer cells will prove critical in transforming cancer prognoses again from chronic disease to cure. The central role played by diagnostic imaging in monitoring therapeutic response dictates that this ability will be predicated on the capability to detect latent disease *in vivo*. However, conventional imaging approaches detect features of active tumors, such as tumor growth and vascularity, but have a demonstrated deficiency in the ability to distinguish tumor necrosis from latent cancer (1,5,6).

The response of hepatocellular carcinoma (HCC) following treatment with transarterial embolization (TAE) provides a compelling example of this important clinical deficiency. TAE, the most common treatment for HCC in the United States (7), exploits the vascular biology of HCC to deprive tumors of nutrients through the targeted delivery of embolics (with or without chemotherapy) to the hepatic arteries feeding the tumor. The presence of viable tumor cells adjacent to necrotic regions on histopathology of explanted tumors following TAE underscores the adaptive response of HCC to nutrient deprivation (8). This adaptive response may result in the observed clinical imaging phenotype of latent HCC surviving TAE that is undetectable using current clinical imaging approaches leading to frequent local recurrences that occur within months of treatment after a complete response. As a result, current imaging paradigms fail to guide optimal therapy by informing the need for repeat interventions (6). Several approaches have been applied in attempts to overcome this limitation including contrast-enhanced (CE) CT (9), CEMRI (10), and diffusion-weighted MRI (11). However, these measurements may be confounded by the replacement of necrotic tissue with healthy liver parenchyma, the presence of iodized oils on CECT, or granulation tissue on CEMRI. Furthermore, these strategies do not provide direct measures of cellular viability. This deficiency reflects a fundamental mismatch between conventional imaging approaches and the biology they seek to characterize, emphasizing the need for functional imaging paradigms to detect latent cancer.

Previously, we demonstrated that HCC cells surviving TAE-like ischemia activate, and are dependent on, a metabolic stress response underscoring the primary role of altered tumor metabolism in their survival (12). These data indicate that the changes in overall metabolic flux and intratumoral metabolites associated with the adapted metabolic equilibrium in latent tumor cells may constitute a unique fingerprint that enables their detection. While ^{18}Fluorodeoxyglucose Positron Emission Tomography (^{18}F-FDG-PET) has revolutionized cancer imaging by leveraging the increased glucose utilization that characterizes many cancers to facilitate detection, it has limited potential for multi-parametric measurement and is not effective in all tumor types, including one third of HCCs (13,14). Nuclear magnetic resonance spectroscopic imaging (MRSI) enhanced by dynamic nuclear polarization (DNP) enables detailed assessments of metabolism *in vivo*. This technology represents a unique resource to translate advances in our understanding of the metabolic alterations enabling cancer latency for non-invasive diagnostic imaging. Through signal enhancement, DNP-^{13}C-MRSI enables simultaneous spatial and kinetic readouts of metabolic activity in near real-time (15). Herein, we describe the characterization of metabolic alterations in latent HCC cells surviving TAE-induced ischemia to enable a sensitive and specific DNP-^{13}C-NMRS imaging approach for the non-invasive detection of latent cancer cells *in vivo*.

RESULTS

Post-TAE-Ischemia Induces Latency In Vivo and In Vitro

In order to characterize ischemia-induced tumor latency, we performed TAE in an autochthonous, diethylnitrosamine (DEN)-induced rat model of HCC as described previously (16,17). Treated tumors demonstrated a marked reduction in volumetric growth relative to untreated controls (n=3/group, Figure 1 A–C), consistent with clinical observations. As compared to untreated tumors, histologic staining of treated tumors demonstrated regions of sustained viability with viable cells showing a decrease in proliferative status as indicated by reduced staining for proliferating cell nuclear antigen (PCNA). This finding was accompanied by the activation of a metabolic stress response as indicated by an increase in the stabilization of hypoxia-inducible factor 1α (Figure 1D, E). The juxtaposition of growth-arrested, latent cancer cells amongst necrotic cells underscored the adaptive response of HCC to nutrient deprivation, which current imaging techniques fail to detect.

To characterize the metabolic alterations of latent HCC cells, we validated an *in vitro* model of TAE-like ischemia based on these *in vivo* data. Rat HCC (HR2) cells, derived from autochthonous, DEN-induced HCCs in Wistar rats, were cultured under nutrient-limiting conditions. Consistent with our previously described data in human HCC cell lines, rat HR2 cells incubated under severe ischemia (1% O_2 with medium containing 1% serum, 1 mM glucose and 0.5 mM glutamine) mimicked the post-TAE *in vivo* growth delay, demonstrating sustained viability for up to one week without proliferation (Supp. Fig. 1A, B). Interestingly, in experiments designed to mimic the revascularization that follows TAE, cells incubated under severe ischemia for one week were then incubated under replete conditions. HR2 cells regained an exponential growth kinetic consistent with the clinical imaging phenotype of recurrent HCC following a period of latency after TAE (Supp. Fig.

1A, B). Consistent with our previously described data in human HCC cell lines, latent HR2 cell populations surviving severe ischemia demonstrated a significant increase in the fraction of non-proliferating cells with 55.4 ± 3.1% of cells in the G_0 phase of the cell cycle versus 18.2 ± 1.1% of cells incubated under standard conditions (Supp. Fig. 1C, D; p<.0001). Latent HCC cells also demonstrated a significant decrease in the fraction of cells in the S phase of the cell cycle (8.4 ± 1%) as compared to cells grown under standard conditions (18.3 ± .4%) in keeping with a reduced proportion of actively dividing cells (Supp. Fig. 1C, D; p=.001). Taken together, these data indicate that ischemia induces a latent and quiescent HCC cell population. This finding was corroborated by increased expression of the cyclin-dependent kinase inhibitor $p27^{Kip1}$ in HR2 cells, as we have demonstrated previously in human HCC cell lines (Supp. Fig. 1E). Consistent with the above-described *in vivo* data, latent HCC cells demonstrated an increase in stabilization of HIF-1α *in vitro* (Supp. Fig. 1E).

Latent HCC Cells Are Hypometabolic

These data indicate that HCC cells surviving severe ischemia suppress their metabolism and proliferative rate to enable latency. Indeed, HCC cells surviving severe ischemia demonstrated biochemical and molecular alterations consistent with the hypometabolic state seen in latent cancer cells. These cells exhibited activation of AMPK, a master cellular energy sensor that inhibits ATP-consuming anabolic programs and activates ATP-producing catabolic programs, as well as downregulation of mTOR pathway activity, as evidenced by decreased Phospho-S6 despite equivalent levels of mTOR, which stimulates ATP-consuming anabolic processes (Fig. 2A). Consistent with these findings, latent HCC cells demonstrated profound reductions in the anabolic metabolism that promotes cancer cell growth including nucleotide, lipid and protein biosynthesis (Fig. 2B, C). HR2 and SNU-387 cells were incubated in either complete or ischemic medium conditions for 48 hours and cell extracts were submitted for global metabolomic profiling. Among the many changes observed in ischemic cells compared to their controls, we identified significantly decreased levels of intermediates of purine and pyrimidine biosynthesis (Fig. 2B). These changes were seen despite elevated levels of orotate, an important precursor, indicating that limited phosphoribosyl pyrophosphate (PRPP) availability due to reduced glucose carbon flux through the pentose phosphate pathway may be the cause of reduced purine and pyrimidine biosynthesis. Similarly, latent HCC cells demonstrated a significant reduction in de novo lipogenesis and protein synthesis (Fig. 2C). Each of these metabolic alterations indicate a concerted shift away from cell growth.

Latent HCC Cells Undergo Metabolic Reprogramming to Enable Survival Under Severe Ischemia

These alterations suggest that latent HCC cells surviving severe ischemia effect a deliberate agenda of metabolic reprogramming to enable survival. To test this hypothesis, we performed unbiased proteomic profiling of HR2 cells incubated under standard and ischemic conditions with a stable isotope of glucose (U-$^{13}C_6$-glucose). Consistent with the data described in Fig. 2C, these data demonstrated a significant reduction in proteins synthesized from glucose (Fig. 3A); however, while global translation was reduced, we also queried the global proteome to identify proteins that increased, rather than decreased under ischemia.

Remarkably, higher peptide levels were detected for almost all enzymes directly involved in glycolysis in HCC cell populations grown under ischemia compared to HCC cells grown under standard conditions (Fig. 3B). This increase in the synthesis of glycolytic enzymes was accompanied by translational and post-translational alterations in the enzymes that metabolize pyruvate in the final step of glycolysis (Fig. 3C). Western blots for these proteins demonstrated increases in the levels of lactate dehydrogenase A (LDHA) and the activated, phosphorylated form of LDHA as well as inactivation of pyruvate dehydrogenase through phosphorylation in HCC cells surviving severe ischemia (Fig. 3C). In addition, these cells demonstrated an increase in the levels of pyruvate carboxylase, likely on the basis of anapleurosis, while no change was observed in the levels of glutamic-pyruvic transaminase (GPT), aka alanine aminotransferase (ALT)). Consistent with these data, while these alterations were associated with a reduction in glucose uptake (Fig. 3D), latent HR2 cells surviving severe ischemia demonstrated an increase in conversion of glucose to lactate relative to alanine as compared to cells grown under standard conditions (Fig. 3E, 18). Indeed, latent HCC cells were dependent on this metabolic reprogramming as demonstrated by the necessity of LDH for survival. The chemical inhibition of LDH (LDHi, 2.5 μM) resulted in the near complete abrogation of lactate synthesis in HR2 cells grown under standard and ischemic conditions (Fig. 3F). However, while cells cultured under standard conditions with LDHi demonstrated persistent growth and viability, cells cultured under ischemic conditions with LDHi failed to maintain viability beyond 48 hours (Fig. 3G) (19,20). Taken together, these data demonstrate that HCC cells surviving TAE-like ischemia cells undergo metabolic reprogramming of glycolysis to shunt glucose carbons away from anabolic processes and towards lactate (Fig. 3H). These findings suggest that metabolic imaging of pyruvate metabolism may provide the sensitivity required to detect this latent cell population.

DNP-13C-NMR Spectroscopy and Spectroscopic Imaging Enable Detection of Latent HCC Cells In Vitro and In Vivo

To test the potential to leverage this metabolic reprogramming for detection of latent HCC cells using hyperpolarized 1-^{13}C-pyruvate, we developed an NMR-compatible, radial flow, cell perfusion bioreactor. HR2 cells were initially perfused with normoxic (0.21 mM/L [21%] O2), standard medium demonstrated increasing oxygen utilization with increases in the nucleoside triphosphate to inorganic phosphate (NTP/P_i) ratio consistent with sustained proliferation (Fig. 4A, B). To mimic the ischemic microenvironment induced by TAE, cells were subsequently perfused with anoxic, nutrient depleted medium (1 mM glucose, 1% FBS and 0.5 mM glutamine) for six hours followed by hypoxic (0.017 mM/L (1.7%) O_2), nutrient depleted medium. Concurrent measurements of O_2 utilization and cellular bioenergetics through ^{31}Phosphorus NMRS demonstrated a marked reduction in oxygen utilization with an associated reduction in the NTP/P_i ratio. Interestingly, a subsequent small increase in the inlet oxygen concentration resulted in an increase in oxygen utilization and a delayed increase in the NTP/P_i ratio, confirming that the capacity for metabolic activity was maintained after exposure to severe O_2 deprivation (Fig. 4A, B). DNP-MRS of hyperpolarized 1-^{13}C-pyruvate enabled the real time assessment of metabolic reprogramming in HCC cells surviving severe ischemia demonstrating a significant reduction in the alanine-to-lactate ratio (Fig. 4C, D).

To assess the capability of DNP-MRSI to leverage this metabolic reprogramming in order to detect latent, treatment-refractory cellular domains *in vivo*, we performed additional experiments using our rat model of autochthonous HCC and TAE. MR imaging demonstrated characteristic features of HCCs in each animal based on the Liver Imaging and Reporting Data System (LI-RADS) that is used to classify liver lesions in the clinic including arterial phase enhancement and washout of this enhancement on delayed phase images (n=3; Fig. 5A)(21). As determined using the modified Response Criteria in Solid Tumors (mRECIST) that are commonly applied to determine therapeutic effect in patients following TAE, each treated HCC (n=6) demonstrated imaging features consistent with a complete radiographic response including a decrease in tumor volumes at day 7 and 14, as well as the disappearance of mass-like intratumoral arterial phase enhancement (APCE) in the target lesion in keeping with a non-viable tumor (n=3, Fig. 5B, C)(18). While four of six treated animals demonstrated persistent radiographic findings of non-viability throughout the tumor for 14 days including stable or reduced size and/or the absence of APCE following TAE, peripheral recurrence was observed after day 4 in two animals identified based mRECIST criteria (Fig. 5C). Interestingly, DNP-MRSI of hyperpolarized 1-^{13}C-pyruvate enabled the detection of viable cellular domains that were undetectable using conventional, contrast-enhanced MR imaging in combination with mRECIST criteria (Fig. 5C–F). Despite the absence of growth within the tumor and/or detectable APCE, quantitative analysis of spectroscopic images demonstrated reduced, but persistent, delivery of pyruvate and metabolism to alanine and lactate in regions of tumors considered non-viable based on mRECIST criteria (Fig. 5D–F). Importantly, and consistent with the metabolic reprogramming observed in our *in vitro* studies of HCC cells surviving severe, TAE-like ischemia, these non-viable tumor regions demonstrated a significant reduction in the alanine-to-lactate ratio following embolization when adjusted for pyruvate levels, as indicated by significant reductions in the coefficient for the generalized regression model (Fig. 5H). In addition, H&E staining of tumors explanted 14 days following TAE demonstrated persistent viability adjacent to regions of necrosis. In tumors regions that were non-viable based on conventional imaging criteria, there was a significant correlation between the levels of intratumoral pyruvate and percent tumor viability at 14 days following embolization (Fig. 5G, I; rho=0.95, p=0.004). In these regions, histologic viability at day 14 was negatively associated with the change in alanine-to-lactate ratio from day 0 to day 14 (Fig. 5J; rho=−0.83, p=0.04). These data indicate that persistent perfusion in combination with metabolic reprogramming are required to enable the survival of HCC under TAE-induced ischemia. Together, these radiographic and histologic findings demonstrate the capability of DNP-MRSI to leverage metabolic reprogramming in order to overcome the limitations of conventional imaging strategies and detect latent, treatment-refractory cellular domains in HCC following TAE.

DISCUSSION

The presented data demonstrate that latent HCC cells utilized metabolic reprogramming to survive the ischemic conditions induced by TAE, altering expression of glycolytic enzymes to reduce anabolic synthesis and increase lactate production. DNP-^{13}C-MRSI was leveraged to identify these metabolic alterations *in vivo* through quantification of 1-^{13}C-alanine

production relative to 1-^{13}C-lactate production following DNP-1-^{13}C-pyruvate administration. This strategy enables the detection of hitherto indiscernible, treatment-refractory cells. These findings address a fundamental deficiency in conventional clinical imaging paradigms for detecting treatment-refractory, latent cellular domains in the poorly perfused microenvironments induced through TAE by applying an innovative approach to the development of imaging biomarkers tailored to the underlying cellular biology.

The integration of the functional measures of metabolism provided by DNP-^{13}C-MRSI in combination with the enhanced glycolytic flux through lactate dehydrogenase in cells surviving severe ischemia overcomes important sensitivity constraints of current imaging paradigms that limit the effectiveness of mRECIST for detecting latent disease. Firstly, these criteria specify a complete imaging response as the absence of residual viable tumor based on the lack of intratumoral contrast enhancement within target lesions on arterial phase imaging (i.e. increased signal due to contrast leaving the arteries and entering the tumor tissue, 21). However, a minority of lesions undergo complete necrosis and local recurrence of HCC has been shown to be common after a complete imaging response (23). Indeed, our finding that severe ischemia induces cellular quiescence in surviving HCC cells provides a potential mechanism to explain the clinical phenotype of recurrent disease in the setting of a complete imaging response. Together, these findings indicate that the absence of intratumoral contrast enhancement denotes tissue ischemia with variable necrosis underscoring the limited sensitivity of contrast enhancement on MRI for the detection of tissue-level vascular patency. In each embolized animal, the enhanced sensitivity afforded by DNP-^{13}C-MRSI enabled the detection of intratumoral 1-^{13}C-pyruvate despite the absence of intratumoral arterial-phase contrast enhancement. Secondly, while the intratumoral delivery of 1-^{13}C-pyruvate demonstrates persistent perfusion following TAE, functional imaging biomarkers are required for the direct detection of viable cell populations. As demonstrated by our data, the detection of latent cancer cells represents a unique challenge with respect to sensitivity given their hypometabolic state and limited number. Indeed, HCC cells surviving TAE-like ischemia demonstrated the abrogation of anabolism with an associated reduction in glucose uptake. The shunting of glucose carbons toward lactate provides an opportunity to overcome sensitivity limitations by leveraging this alteration for functional metabolic imaging. DNP-^{13}C-MRSI enabled the direct detection of surviving HCC cells based on their uptake of 1-^{13}C-pyruvate and metabolism to 1-^{13}C-lactate and 1-^{13}C-alanine. The serial measurement of individual metabolites enables the assessment of metabolic flux providing a unique imaging biomarker that is not accessible through other non-invasive imaging modalities and may be integrated with FDG-PET to allow for a more complete characterization of tumor metabolism (24,25). Moreover, the positive association of cellular viability following TAE with pyruvate levels as well as the negative association of viability with alanine-to-lactate ratios suggest that DNP-^{13}C-MRSI may be utilized to establish quantitative metrics that predict treatment response and enable interpatient comparisons.

Importantly, the ability to detect treatment-refractory, latent HCC cells following TAE holds important implications for improving outcomes in patients by informing both the timing and type of subsequent therapy. Indeed, optimal therapy with TAE is limited by current imaging measures of residual disease, which fail to guide repeat interventions that may mitigate recurrence and/or metastasis. This opportunity is underscored by the fact that a maximal

response with TAE is observed following several interventions as well as preclinical data demonstrating that HCC cells surviving TAE-induced ischemia have an increased propensity for invasion and metastasis (26,27). In addition to improving treatment response through earlier re-treatment, the ability to identify treatment-resistant, latent HCC cells following TAE may overcome limitations of adjunct therapies administered at the time of TAE by informing the selection of these agents. Prospective, randomized trials demonstrate no difference between TAE or TAE in combination with the intra-arterial delivery of chemotherapy (TACE) with respect to survival. These data underscore the failure of currently administered TACE agents, which include cell-cycle specific chemotherapeutics targeting proliferating cancer cells, to potentiate the cytotoxicity of embolotherapy-induced ischemia (28–31). We, and others, have shown that the ischemic microenvironment generated by TAE induces dependencies on metabolic stress responses (MSR) in surviving HCC cells including autophagy (12,32). These data suggest that the detection of HCC cells surviving poorly perfused, ischemic microenvironments using DNP-^{13}C-MRSI of hyperpolarized 1-^{13}C-pyruvate will enable this constrained phenotype to be leveraged by selecting therapeutics that specifically target MSR dependencies such as autophagy inhibitors (12). These findings provide the rationale for a phase 1–2 clinical trial studying the application of DNP-^{13}C-MRSI of hyperpolarized 1-^{13}C-pyruvate to assess response to combination therapy using the autophagy inhibitor hydroxychloroquine with TACE for the treatment of unresectable HCC.

The described studies applied a translational approach that enhance the likelihood of clinical application. The animal model used for these studies has been validated as a translational model of autochthonous HCC and TAE through several publications (12,16,17). Specifically, the model recapitulates the progression of the human disease wherein patients develop cirrhosis followed by HCC. The TAE procedure precisely mimics the procedure performed in humans including selective embolization of autochthonous tumor feeding vessels. In addition, DNP-^{13}C-MRSI is a clinically relevant technology with established protocols for generating hyperpolarized substrate for injection into animals and humans through a published clinical trial as well as the commercial availability of pre-prepared hyperpolarized 1–13C-pyruvate flow paths (24,33–35). The concentrations of hyperpolarized 1–13C-pyruvate used for this study match those used for patients. In addition, the polarization efficiency of clinical hyperpolarizers (~50%) is significantly higher than the preclinical hyperpolarizer used in our studies (~30%) enabling a substantial increase in signal-to-noise. Moreover, the scan time required for the acquisition of DNP-^{13}C-MRS images is a fraction of that required for the acquisition of conventional MR images. As such, these images can be acquired in the context of current clinical imaging workflows. Given the fact that the spin-lattice relaxation times are shorter at lower field strengths, the acquisition of hyperpolarized images at field strengths used in the clinic (1.5 and 3.0T) will result in improved image quality due to the longer lifetime of the hyperpolarized spin state.

In summary, the characterization of ischemia-induced metabolic reprogramming in HCC cells enabled the development a DNP-^{13}C-MRS imaging strategy to detect latent, latent cellular domains following TA(C)E. This approach emphasizes the power of integrating unique aspects of cancer biology with functional imaging technologies to address deficiencies in conventional imaging paradigms.

MATERIALS AND METHODS

Cell Lines, Cellular Growth Kinetics and Cell Cycle Analyses

Human HCC cell lines were obtained from American Type Culture Collection (HepG2, SNU-449 and SNU-387 Manassas, VA) or Sekisui XenoTech (Huh7, Kansas City, MO). Each cell line was maintained in RPMI medium with 0.3 g/L L-glutamine supplemented with 1.8 g/L D-glucose, 20 mM HEPES, 2 g/L sodium bicarbonate and 10% FBS. Rat hepatocellular carcinoma cells (HR-2) derived from diethylnitrosamine (DEN)-induced HCCs in Wistar rats were a generous gift from Dr. Istvàn Blazsek of Paul Brousse Hospital, Villejuif, France (36). HR-2 cells were maintained in DMEM medium (DMP52–1LT; Caisson Laboratories, Inc.; Smithfield, UT) supplemented with 3 g/L glucose, 20 mM HEPES, 3.7 g/L Sodium Bicarbonate and 10% FBS. The incubation medium was exchanged for fresh medium every 48 hours. Cellular growth kinetics and cell cycle states were measured as described previously and in the Supplementary Materials and Methods (12).

Metabolomic Profiling

Unlabeled metabolite profiling was performed using a YSI 2950D Biochemistry Analyzer (Yellow Springs, Ohio) according to the manufacturer's instructions. Labeled metabolite profiling was performed on perchloric acid extracts of HR2 cells incubated for 48 hours with U-^{13}C-glucose under standard or ischemic conditions. Pan metabolomic profiling was performed on HR2 cells incubated for 48 hours under standard or ischemic conditions in collaboration with Metabolon (Morrisville, NC). Details regarding the experiments utilized for unlabeled metabolite profiling, labeled metabolomic profiling, pan metabolomic profiling, western blot generation, and labeled proteomic profiling are available in the Supplemental Materials and Methods.

Protein/Proteomic Profiling

Western Blot Analysis: Western blog analyses were performed as described previously and in the Supplementary Materials and Methods (12).

Labeled Proteomic Profiling: HR2 cells were grown as described above for the labeled profiling experiments. After 48 hours of growth, the medium was exchanged for medium containing U-C^{13}-Glucose-labelled at the relevant concentration. After 24 additional hours of incubation, the cells were scraped and pelleted with a small sample utilized to acquire cell counts for normalization purposes. Proteins were subsequently extracted from the cell pellets using standard methodologies and eluted protein solutions were then dried and reconstituted with 8M urea. Denaturation/reduction of the sample was performed in 8 M urea/5 mM dithiothreitol/25 mM NH_4HCO_3 (pH 8.0) for over 60 minutes at 52°C. The solution was stored at room temperature in 25 mM iodoacetamide at the dark for 60 min. The urea was diluted to a concentration of 1 M with 25 mM NH_4HCO_3 and then digested with trypsin (1:50 ratio) at 37°C and shaking for 16 hrs. Prepared samples were subsequently analyzed as described in the Supplementary Materials and Methods.

Immunohistochemistry—For proliferation and HIF-1α analyses, standard immunohistochemistry protocols were used to stain formalin-fixed, paraffin-embedded tissues as described in the Supplementary Materials and Methods.

Autochthonous rat model of HCC and TAE—Animal studies were conducted according to institutionally approved protocols for the safe and humane treatment of animals. Autochthonous HCCs were induced in male Wistar rats using an established protocol including ad libitum oral intake of 0.01% diethylnitrosamine (DEN) for 12 weeks[16]. Rats with tumors 0.5–1.0 cm in maximal diameter on T_2-weighted MRI were selected for treatment. Using fluoroscopic guidance, segmental catheterization and embolization with 0.1 mL of 40–120 μm Embosphere particles (Merit Medical, South Jordan, Utah) diluted in 0.1 mL iopamidol contrast medium (Isovue 370; Bracco, Monroe Township, New Jersey) was performed as described previously[16]. Pre- and post-embolization arteriography was performed using an AngioStar Plus Imaging System (Siemens, Malvern, Pennsylvania).

Dynamic Nuclear Polarization ^{13}Carbon Magnetic Resonance Spectroscopy and Spectroscopic Imaging

DNP of 1-^{13}C-pyruvate: Dynamic Nuclear Polarization of 1-^{13}C-pyruvate was performed using a HyperSense DNP polarizer (Oxford Instruments, Abingdon, UK) at an excitation frequency of 94.080 GHz and temperature of ~1.4 K. DNP was performed on a stock mixture of 14 M [1-^{13}C]-pyruvate (Cambridge Isotopes, Tewksbury, MA), 15 mM OX063 radical (GE Healthcare) and 1.5 mM of Dotarem (Guerbet LLC, Princeton, NJ). 22 μL of stock solution were melted in 4 mL or 8 mL of dissolution buffer (80 mM NaOH, 40 mM Trizma (pH = 7.6), 50 mM NaCl and 0.42 mM EDTA), for *in vivo* or *in vitro* experiments for *in vivo* or *in vitro* experiments respectively, at 10-bar pressure and 180 °C to yield 80 mM isotonic, neutral hyperpolarized 1-^{13}C-pyruvate. For *in vitro experiments*, 6.3 mL of hyperpolarized 1-^{13}C-pyruvate was pumped into the cell mass at 7 mL/min. For *in vivo* studies, 6.7 mL/kg of the sample was administered through a tail vein catheter over 13 seconds by hand injection, followed by administration of 300-μL saline over 2 seconds to flush the pyruvate from the catheter's dead volume.

MRS: MR spectroscopy was performed on perfused HR-2 cells inside an Oxford 9.4 Tesla, 8.9 cm bore magnet interfaced to an Agilent Direct Drive Console (Wilmington, DE). The cell perfusion apparatus used to perfuse cells inside the NMR spectrometer was similar to that described previously with modifications to maintain carefully controlled hypoxic conditions and the injection of hypoxic hyperpolarized substrates (37). These modifications included the design of a radial flow bioreactor (manuscript in preparation) as well as the addition of the Oxycyte perfluorocarbon (5%, Aurum Biosciences, Glasgow, UK) to the perfusion medium for ischemic conditions. The NMR tube contained a packed bed of microcarriers that was continuously perfused with cell culture medium. In-line polarographic oxygen probes (Mettler-Toledo, Columbus, OH) were used at the inlet and outlet of the NMR tube. A 20-mm broadband liquids probe was used to acquire ^{31}P and ^{13}C spectra (Doty Scientific: Columbia, SC). For ^{31}P spectra, 60^{o} pulses were used with a repetition time of 1000 ms. For ^{13}C NMR, spectra were acquired with 12^{o} pulses to limit

radiofrequency-induced relaxation of the hyperpolarized spin state, a repetition time of 3 s, 8192 points, and a spectral width of 25000 Hz. WALTZ-16 decoupling was used during signal acquisition to improve spectral resolution. Resonance intensities were determined with MestreNova NMR software.

MRI and MRSI: MR images were acquired using an Agilent 4.7T, 40 cm horizontal bore MR Spectrometer with a 25 gauss/cm gradient tube interfaced to an Agilent DirectDrive console. Each animal was positioned within a Polarean proton-tuned (200.1 MHz) birdcage resonator with quadrature polarization with a Polarean ^{13}Carbon-tuned (50.525 MHz) surface coil positioned over the right upper quadrant (Polarean: Durham, NC). A detailed description of the parameters used to acquire T_2-weighted and contrast-enhanced T_1-weighted images is included in the Supplementary Materials & Methods. DNP-^{13}C-MRSI was acquired using a 2D (slab thickness = 10 mm) echoplanar spectroscopic imaging (EPSI) sequence and a spectral bandwidth of 1.1kHz with 128 points, enabling detection of chemical shifts of 22 ppm (38). The FOV was 60 mm x 45 mm with 12 phase encode steps and 16 frequency encode steps, enabling an in-plane resolution of 3.75 mm x 3.75 mm. This sequence required ~2 s to complete and was repeated every ~4 s for a minimum of 10 scans per study. Image acquisition was initiated 25 s following the commencement of the injection to maximize the observed lactate signal. Data were processed and analyzed as described in the Supplementary Materials and Methods.

Histology

Treated and untreated tumors were harvested from rats following CO_2 euthanasia using institutionally approved protocols. Tissues were subsequently formalin fixed for staining and the percentage of viable HCC was estimated from hematoxylin and eosin (H&E) stained sections by a hepatobiliary pathologist with extensive experience in HCC (EEF).

Statistical analyses

Statistical analyses were performed with the use of GraphPad Prism version 6.02 (GraphPad Software, San Diego, CA), R 3.4.4, and STATA 15. Tumor viability is reported as the average percent viability of all targeted tumors on H&E stained histologic sections. Mean values are reported as mean ± SD of the mean. Data were analyzed using the Shapiro-Wilk test for normality. For normally distributed data, two-tailed *t* test was performed to assess the statistical significance of differences in mean values. For the case of individual metabolite levels before and after embolization, data were not normally distributed, and the Wilcoxon signed rank test was used to compare metabolite measures between time points. Quasi-least squares (QLS) regression was used to model the alanine-to-lactate ratio over time adjusted for pyruvate. The regression models were implemented using the xtqls function in STATA 15.0. QLS is an alternative method for estimating the correlation parameters within the framework of the generalized estimating equation (GEE) approach. This approach allows for implementation of the autoregressive correlation structure among repeated measures that are unequally spaced in time.

Data availability

The datasets generated during and/or analyzed during the current study are available from the corresponding author on reasonable request.

Code availability

The code used during the current study are available from the corresponding author on reasonable request.

Supplementary Material

Refer to Web version on PubMed Central for supplementary material.

ACKNOWLEDGEMENTS

The authors thank Len Neckers and the NCI Experimental Therapeutics program for the development and provision of the 737 LDH inhibitor.

Financial support: This study was supported in part by the National Institutes of Health, Director's Office, Grant DP5OD021391 (TPG) as well as the Institute for Translational Medicine and Therapeutics of the University of Pennsylvania and the Society for Interventional Radiology Foundation (TPG). The project was supported in part by the National Center for Research Resources Grant UL1RR024134 and is now at the National Center for Advancing Translational Sciences, Grant UL1TR000003 (TPG).

REFERENCES

1. Stegmeier F, Warmuth M, Sellers WR, Dorsch M. Targeted cancer therapies in the twenty-first century: lessons from imatinib. Clin. Pharmacol. Ther. 2010;87:543–552. [PubMed: 20237469]
2. Pfitzenmaier J, Ellis WJ, Arfman EW, Hawley S, Mclaughlin PO, Lange PH, et al. Telomerase activity in disseminated prostate cancer cells. BJU Int. 2006;97:1309–1313. [PubMed: 16686730]
3. Karrison TG, Ferguson DJ, Meier P. Dormancy of mammary carcinoma after mastectomy. J. Natl. Cancer Inst. 1999;91:80–85. [PubMed: 9890174]
4. Aguirre-Ghiso JA. Models, mechanisms and clinical evidence for cancer dormancy. Nat. Rev. Cancer [Internet]. 2007;7:834–846. Available from: http://eutils.ncbi.nlm.nih.gov/entrez/eutils/elink.fcgi?dbfrom=pubmed&id=17957189&retmode=ref&cmd=prlinks%5Cnpapers2://publication/doi/10.1038/nrc2256 [PubMed: 17957189]
5. Desar IME, van Herpen CML, van Laarhoven HWM, Barentsz JO, Oyen WJG, van der Graaf WT a. Beyond RECIST: Molecular and functional imaging techniques for evaluation of response to targeted therapy. Cancer Treat. Rev. 2009;35:309–321. [PubMed: 19136215]
6. Forner A, Ayuso C, Varela M, Rimola J, Hessheimer AJ, De Lope CR, et al. Evaluation of tumor response after locoregional therapies in hepatocellular carcinoma: Are response evaluation criteria in solid tumors reliable? Cancer. 2009;115:616–623. [PubMed: 19117042]
7. Shah S a., Smith JK, Li Y, Ng SC, Carroll JE, Tseng JF. Underutilization of therapy for hepatocellular carcinoma in the medicare population. Cancer. 2011;117:1019–1026. [PubMed: 20945363]
8. Higuchi T, Kikuchi M, Okazaki M. Hepatocellular Carcinoma after Transcatheter Hepatic Arterial Embolization: A Histopathologic Study of 84 Resected Cases. Cancer. 1994;73:2259–2267. [PubMed: 7513245]
9. Monsky WL, Kim I, Loh S, Li C-SS, Greasby TA, Deutsch L- SS, et al. Semiautomated segmentation for volumetric analysis of intratumoral ethiodol uptake and subsequent tumor necrosis after chemoembolization. Am. J. Roentgenol. 2010;195:1220–1230. [PubMed: 20966331]
10. Kim S, Mannelli L, Hajdu CH, Babb JS, Clark TWI, Hecht EM, et al. Hepatocellular Carcinoma: Assessment of Response to Transarterial Chemoembolization With Image Subtraction. Analysis. 2010;31:348–355.

11. Kamel IR, Bluemke DA, Ramsey D, Abusedera M, Torbenson M, Eng J, et al. Role of Diffusion-Weighted Imaging in Estimating Tumor Necrosis After Chemoembolization of Hepatocellular Carcinoma. Am. J. Radiol. 2003;181:708–710.
12. Gade TPF, Tucker E, Nakazawa MS, Hunt SJ, Wong W, Krock B, et al. Ischemia Induces Quiescence and Autophagy Dependence in Hepatocellular Carcinoma. Radiology. 2017;
13. Pantel AR, Ackerman D, Lee SC, Mankoff DA, Gade TPF. Imaging Cancer Metabolism: Underlying Biology and Emerging Strategies. J. Nucl. Med. 2018;59:1340–1349. [PubMed: 30042161]
14. Chen R, Li J, Zhou X, Liu J, Huang G. Fructose-1,6-bisphosphatase 1 reduces 18F FDG uptake in hepatocellular carcinoma. Radiology. 2017;284:844–853. [PubMed: 28387640]
15. Ardenkjær-Larsen JH, Fridlund B, Gram A, Hansson G, Hansson L, Lerche MH, et al. Increase in signal-to-noise ratio of >10,000 times in liquid-state NMR. Proc. Natl. Acad. Sci. 2003;100:10158–10163. [PubMed: 12930897]
16. Gade TPFF Hunt SJ, Harrison N Nadolski GJNJ, Weber C, Pickup S, et al. Segmental Transarterial Embolization in a Translational Rat Model of Hepatocellular Carcinoma. J. Vasc. Interv. Radiol. [Internet]. 2015;26:1229–1237. Available from: 10.1016/j.jvir.2015.02.006 [PubMed: 25863596]
17. Kiefer RM, Hunt SJ, Pulido S, Pickup S, Furth EE, Soulen MC, et al. Relative Initial Weight Is Associated with Improved Survival without Altering Tumor Latency in a Translational Rat Model of Diethylnitrosamine-Induced Hepatocellular Carcinoma and Transarterial Embolization. J. Vasc. Interv. Radiol. [Internet]. 2017;28:1043–1050. Available from: 10.1016/j.jvir.2017.03.037 [PubMed: 28495453]
18. Lencioni R, Llovet JM. Modified RECIST (mRECIST) assessment for hepatocellular carcinoma. Semin. Liver Dis. 2010;30:52–60. [PubMed: 20175033]
19. Rai G, Brimacombe KR, Mott BT, Urban DJ, Hu X, Yang SM, et al. Discovery and Optimization of Potent, Cell-Active Pyrazole-Based Inhibitors of Lactate Dehydrogenase (LDH). J. Med. Chem. 2017;60:9184–9204. [PubMed: 29120638]
20. Yeung C, Gibson AE, Issaq SH, Oshima N, Baumgart JT, Edessa LD, et al. Targeting Glycolysis through Inhibition of Lactate Dehydrogenase Impairs Tumor Growth in Preclinical Models of Ewing Sarcoma. Cancer Res. 2019;79:5060–5073. [PubMed: 31431459]
21. Mitchell DG, Bruix J, Sherman M, Sirlin CB. LI-RADS (Liver Imaging Reporting and Data System): Summary, discussion, and consensus of the LI-RADS Management Working Group and future directions. Hepatology. 2015;61:1056–1065. [PubMed: 25041904]
22. Llovet JM, Di Bisceglie AM, Bruix J, Kramer BS, Lencioni R, Zhu AX, et al. Design and endpoints of clinical trials in hepatocellular carcinoma. J. Natl. Cancer Inst. 2008;100:698–711. [PubMed: 18477802]
23. Jin Y-J, Chung Y- H, Kim J a, Park W, Lee D, Shim JH, et al. Predisposing factors of hepatocellular carcinoma recurrence following complete remission in response to transarterial chemoembolization. Dig. Dis. Sci. 2013;58:1758–65. [PubMed: 23361574]
24. Day SE, Kettunen MI, Gallagher FA, Hu D-E, Lerche M, Wolber J, et al. Detecting tumor response to treatment using hyperpolarized 13C magnetic resonance imaging and spectroscopy. Nat. Med. [Internet]. 2007;13:1382–1387. Available from: http://www.nature.com/doifinder/10.1038/nm1650 [PubMed: 17965722]
25. Gutte H, Hansen a. E, Larsen M, Rahbek S, Henriksen S, Johannesen H, et al. Simultaneous hyperpolarized 13C-pyruvate MRI and 18F-FDG-PET (HyperPET) in 10 canine cancer patients. J. Nucl. Med. 2015;56:1786–92. [PubMed: 26338899]
26. Liu L, Ren Z-G, Shen Y, Zhu X-D, Zhang W, Xiong W, et al. Influence of hepatic artery occlusion on tumor growth and metastatic potential in a human orthotopic hepatoma nude mouse model: relevance of epithelial-mesenchymal transition. Cancer Sci. 2010;101:120–8. [PubMed: 19832842]
27. Farinati F, De Maria N, Marafin C, Herszenyi L, Del Prato S, Rinaldi M, et al. Unresectable hepatocellular carcinoma in cirrhosis: survival, prognostic factors, and unexpected side effects after transcatheter arterial chemoembolization. Dig. Dis. Sci. 1996;41:2332–9. [PubMed: 9011438]

28. Kawai S, Okamura J, Ogawa M, Ohashi Y, Tani M, Inoue J, et al. Prospective and randomized clinical trial for the treatment of hepatocellular carcinoma--a comparison of lipiodol-transcatheter arterial embolization with and without adriamycin (first cooperative study). The Cooperative Study Group for Liver Cancer Treat. Cancer Chemother. Pharmacol. 1992;31:S1–6.

29. Llovet JM, Real MI, Montaña X, Planas R, Coll S, Aponte J, et al. Arterial embolisation or chemoembolisation versus symptomatic treatment in patients with unresectable hepatocellular carcinoma: a randomised controlled trial. Lancet. 2002;359:1734–9. [PubMed: 12049862]

30. Chang JM, Tzeng WS, Pan HB, Yang CF, Lai KH. Transcatheter arterial embolization with or without cisplatin treatment of hepatocellular carcinoma. A randomized controlled study. Cancer. 1994;74:2449–53. [PubMed: 7922999]

31. Marelli L, Stigliano R, Triantos C, Senzolo M, Cholongitas E, Davies N, et al. Transarterial therapy for hepatocellular carcinoma: which technique is more effective? A systematic review of cohort and randomized studies. Cardiovasc. Intervent. Radiol. 2007;30:6–25. [PubMed: 17103105]

32. Gao L, Song J, Zhang J, Zhao X, Zhao Q, Sun K, et al. Chloroquine promotes the anticancer effect of TACE in a rabbit VX2 liver tumor model. Int. J. Biol. Sci. 2013;9:322–30.

33. Nelson SJ, Kurhanewicz J, Vigneron DB, Larson PEZ, Harzstark AL, Ferrone M, et al. Metabolic imaging of patients with prostate cancer using hyperpolarized [1–13C]Pyruvate. Sci. Transl. Med. 2013;5:1–10.

34. Bohndiek SE, Kettunen MI, Hu D, Witney TH, Kennedy BWC, Gallagher F a, et al. Detection of tumor response to a vascular disrupting agent by hyperpolarized 13C magnetic resonance spectroscopy. Mol. Cancer Ther. 2010;9:3278–88. [PubMed: 21159611]

35. Keshari KR, Wilson DM. Chemistry and biochemistry of 13C hyperpolarized magnetic resonance using dynamic nuclear polarization. Chem. Soc. Rev. 2014;43.

36. Thièry JP, Blazsek I, Legras S, Marion S, Reynes M, Anjo a, et al. Hepatocellular carcinoma cell lines from diethylnitrosamine phenobarbital-treated rats. Characterization and sensitivity to endothall, a protein serine/threonine phosphatase-2A inhibitor. Hepatology. 1999;29:1406–17. [PubMed: 10216123]

37. Mancuso a Beardsley NJ, Wehrli S, Pickup S, Matschinsky FM, Glickson JD. Real-time detection of 13C NMR labeling kinetics in perfused EMT6 mouse mammary tumor cells and betaHC9 mouse insulinomas. Biotechnol. Bioeng. 2004;87:835–48. [PubMed: 15334410]

38. Basic Practical NMR Concepts : A Guide for the Modern Laboratory. Max T. Rogers NMR Facil. 2013;1–41.

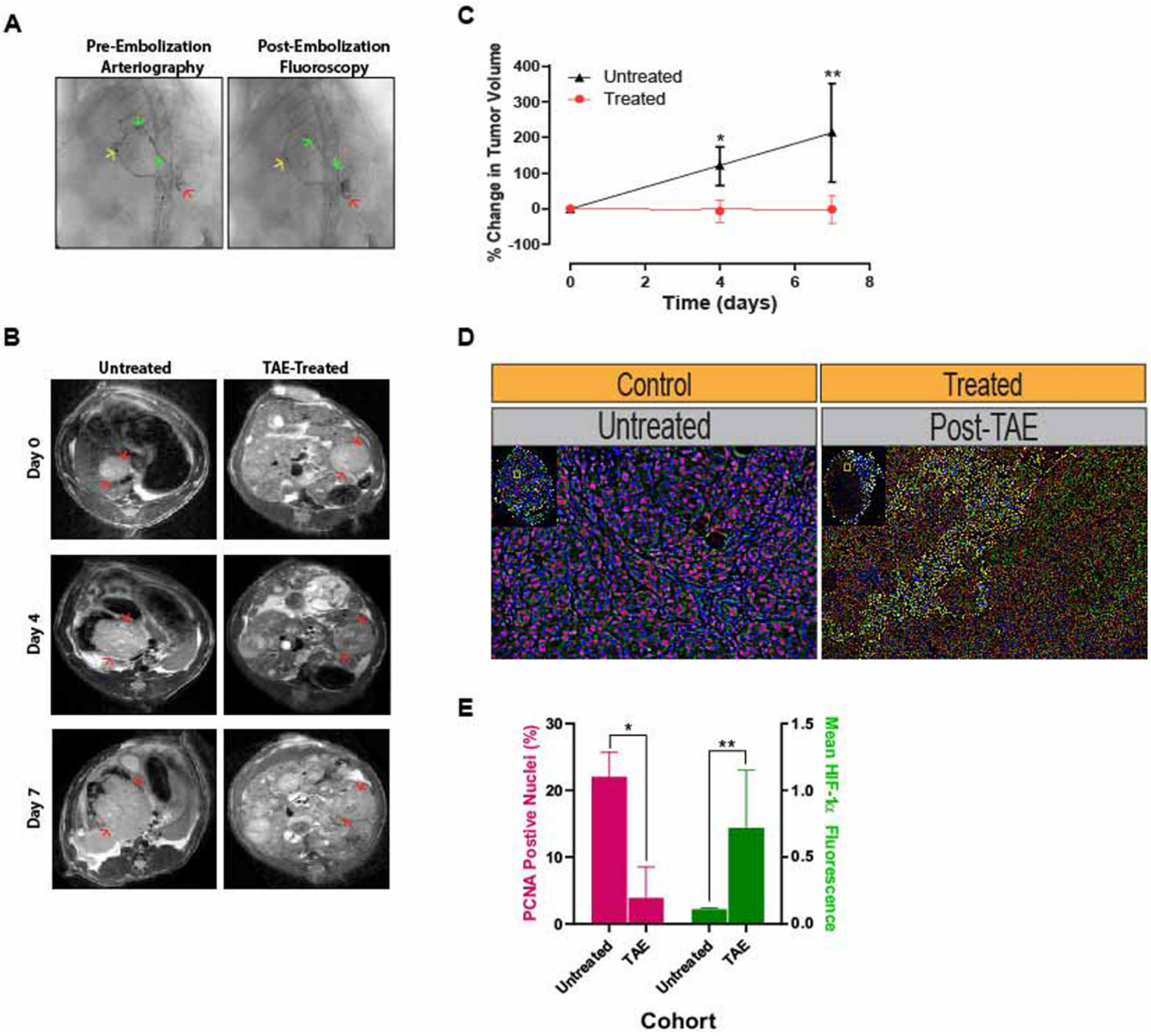

Figure 1. Post-TAE Ischemia Induces Growth Latency *In Vivo*.

(*A*) Representative pre-embolization arteriogram demonstrates positioning of the microcatheter in the left hepatic artery (→) with contrast extending to (→) and staining the tumor (→). Post-embolization fluoroscopy demonstrates stasis of contrast within the left hepatic branch artery feeding the tumor as well as persistent contrast staining the tumor. (*B*) Representative serial T_2-weighted MR images of untreated, control HCCs and treated HCCs prior to and following TAE. (*C*) Growth curves derived from MR-based measurements of tumor volume in untreated HCCs and treated HCCs prior to and following TAE demonstrated a significant reduction in growth for TAE-treated tumors (p=0.011 at posttreatment day 4; p=0.029 at posttreatment day 7)). Tumor volumes are normalized to the first measurement and reported as the average percent change in volume ± standard deviation. (*D*) Representative immunofluorescence images of untreated control and TAE

treated (post-treatment day 7) tumors stained for PCNA (pink) and HIF-1α (green). (*E*) Bar graph demonstrating a significant reduction in the percentage of DAPI+ nuclei that are also PCNA+ in treated tumors relative to untreated tumors as well as an increase in mean HIF-1α fluorescence intensity per DAPI+ stained nucleus (PCNA: 3.9 ± 4.6% vs 22.0 ± 3.7%, p=.006; HIF-1α: .75 ± .39 vs .11 ± .01, p=.048).

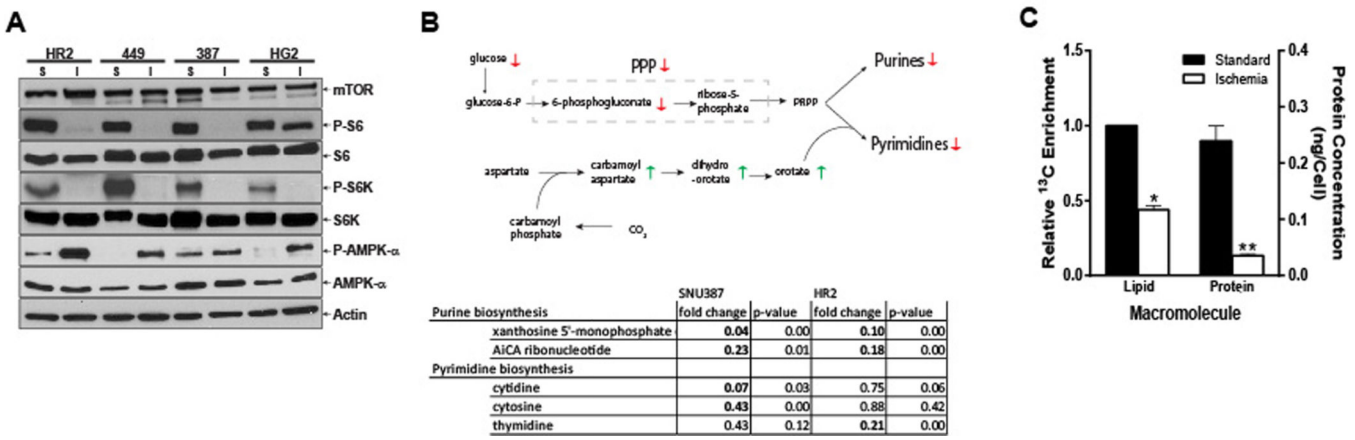

	SNU387		HR2	
Purine biosynthesis	fold change	p-value	fold change	p-value
xanthosine 5'-monophosphate	**0.04**	0.00	**0.10**	0.00
AICA ribonucleotide	**0.23**	0.01	**0.18**	0.00
Pyrimidine biosynthesis				
cytidine	**0.07**	0.03	0.75	0.06
cytosine	**0.43**	0.00	0.88	0.42
thymidine	0.43	0.12	**0.21**	0.00

Figure 2. Latent HCC Cells Are Hypometabolic.

(*A*) Western blots demonstrating suppression of the mTOR pathway, as supported by decreased Phospho-S6 levels despite sustained mTOR levels, and activation of the AMPK pathway in three human HCC (449, 387 and HG2) cell lines and one rat (HR2) HCC cell line exposed to ischemic (I) as compared standard conditions (S). (*B*) Metabolomic profiling of cells grown under ischemic vs. standard conditions demonstrates a reduction in intermediates of purine and pyrimidine biosynthesis in human (SNU387) and rat (HR2) HCC cell lines. (*C*) NMR extracts of HR2 cells incubated with 1-^{13}C-acetate and surviving ischemic conditions demonstrated significant reductions in the synthesis of de novo lipids as compared to cells grown under standard conditions (p=.0013). Similarly, bicinchoninic acid assay protein measurements demonstrated significant reductions in protein synthesis for HR2 cells surviving severe ischemia as compared to cells grown under standard conditions (p=.0086).

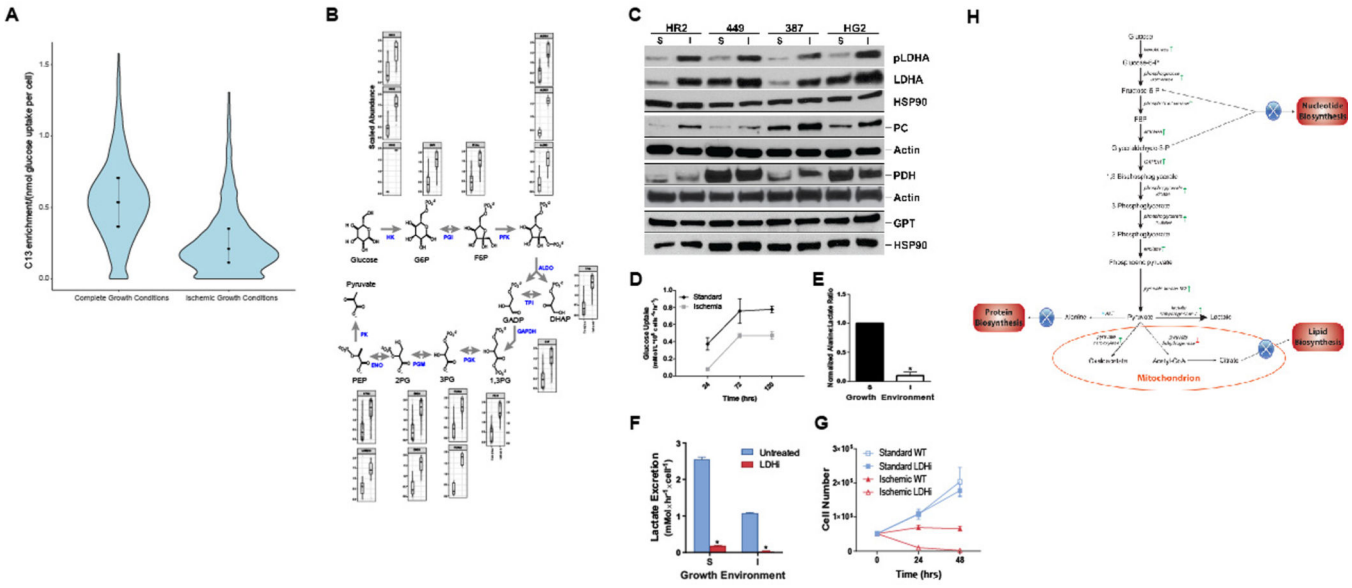

Figure 3. Latent HCC Cells Undergo Metabolic Reprogramming.

(*A*) HR2 cells grown under severe ischemia with U-1-^{13}C-glucose demonstrated lower C13-labeled protein enrichment as compared to cells grown under standard conditions, indicating reduced translation from glucose-derived alanine (p<2.2e-16). (*B*) Abundance of total peptide (C13 and C12 combined) graphed after normalization to mean peptide abundance for all peptides mapping to glycolytic enzymes revealed a consistent increase in abundance of glycolytic enzymes under ischemia, despite overall reduction in translation. (*C*) Western blots demonstrating translational and post-translational alterations in the enzymes that metabolize pyruvate in the final step of glycolysis in cells surviving severe ischemia (I), relative to cells grown under standard conditions (S), including an increase in the levels of LDHA and its activated, phosphorylated form. In addition, phosphorylation of pyruvate dehydrogenase to its inactive form was observed as a band shift toward a higher molecular weight. (*D*) Despite these alterations, metabolic analyses demonstrated a reduction in glucose uptake for cells surviving severe ischemia (p=.0004). (*E*) NMR spectroscopy of cell extracts incubated with glucose demonstrated alterations in glycolytic flux consistent with the above-described changes in protein expression with a significant reduction in the alanine:lactate ratio (p=.03). (*F*, *G*) Chemical inhibition of LDH (LDHi 737, 2.5 μM) resulted in the suppression of lactate excretion for HCC cells grown under standard and ischemic conditions within 24 hours of incubation; however, cells grown under ischemia were unable to survive these conditions when LDH was inhibited (p<0.0001 for comparisons of lactate excretion rate under standard and ischemic conditions). (*H*) Schematic illustrating metabolic reprogramming of HCC cells surviving severe ischemia to limit anabolism and shunt glucose towards carbons toward lactate.

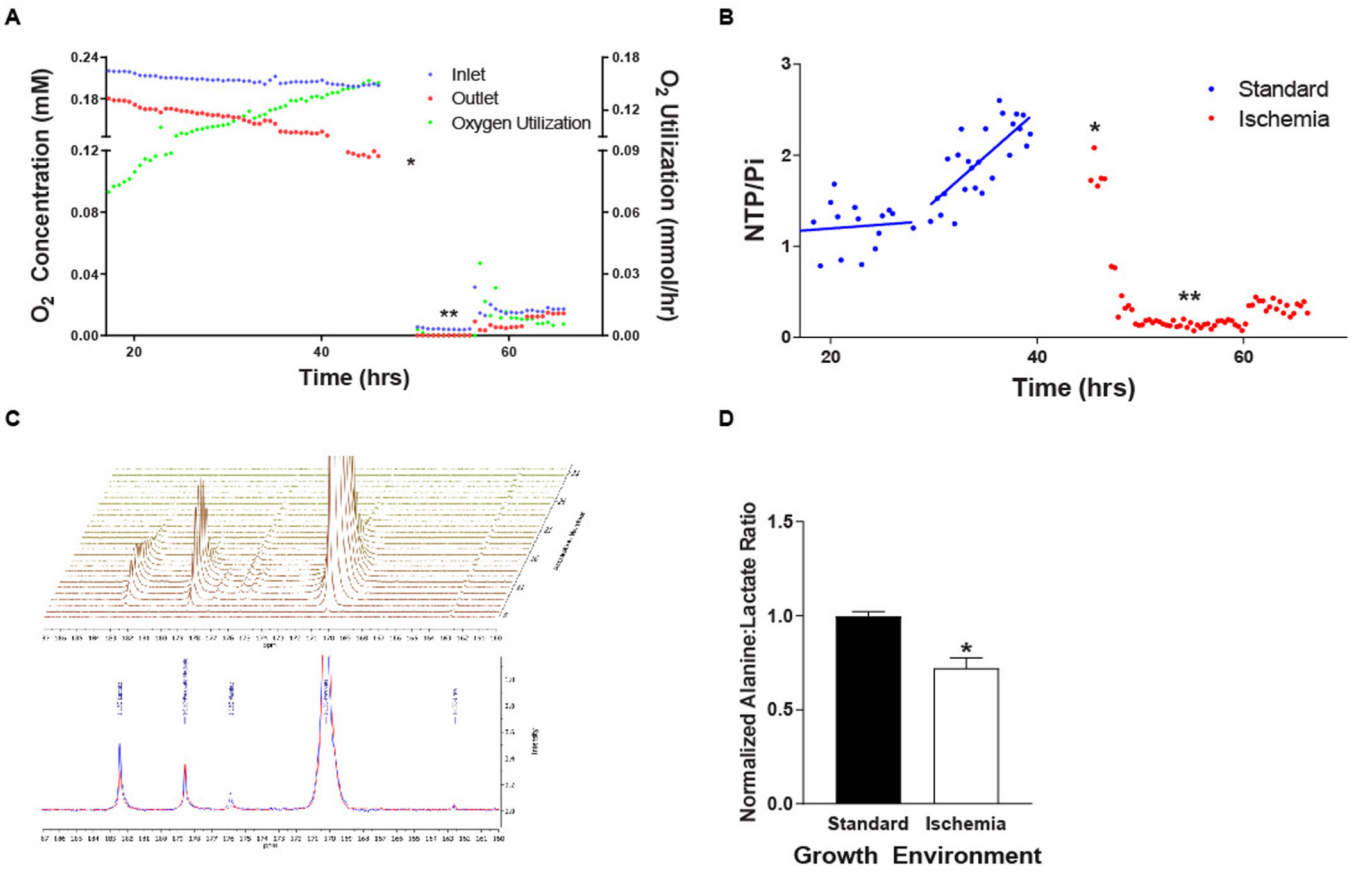

Figure 4. DNP-MRS Demonstrates Metabolic Reprogramming in Perfused HCC Cells Surviving Severe Ischemia *In Vitro*.

(*A*, *B*) HCC cells grown under standard growth conditions demonstrated increasing levels of oxygen utilization and associated nucleoside triphosphate to inorganic phosphate (NTP/P_i) ratios, which diminished rapidly when the growth environment is changed to ischemic conditions (anoxia with nutrient depleted medium, single arrow) for 6 hours mimicking TAE. The maintenance of cellular viability under these conditions was underscored by an increase in the oxygen utilization and the NTP/P_i ratio when the oxygen level is increased to 0.017 mM (double arrow). (*C*, *D*) DNP-MRS of hyperpolarized 1-^{13}C-pyruvate demonstrates metabolic reprogramming of cells surviving TA(C)E-like ischemia (blue spectrum) with a reduction in the alanine to lactate ratio (n=2 injections per condition; p=.023).

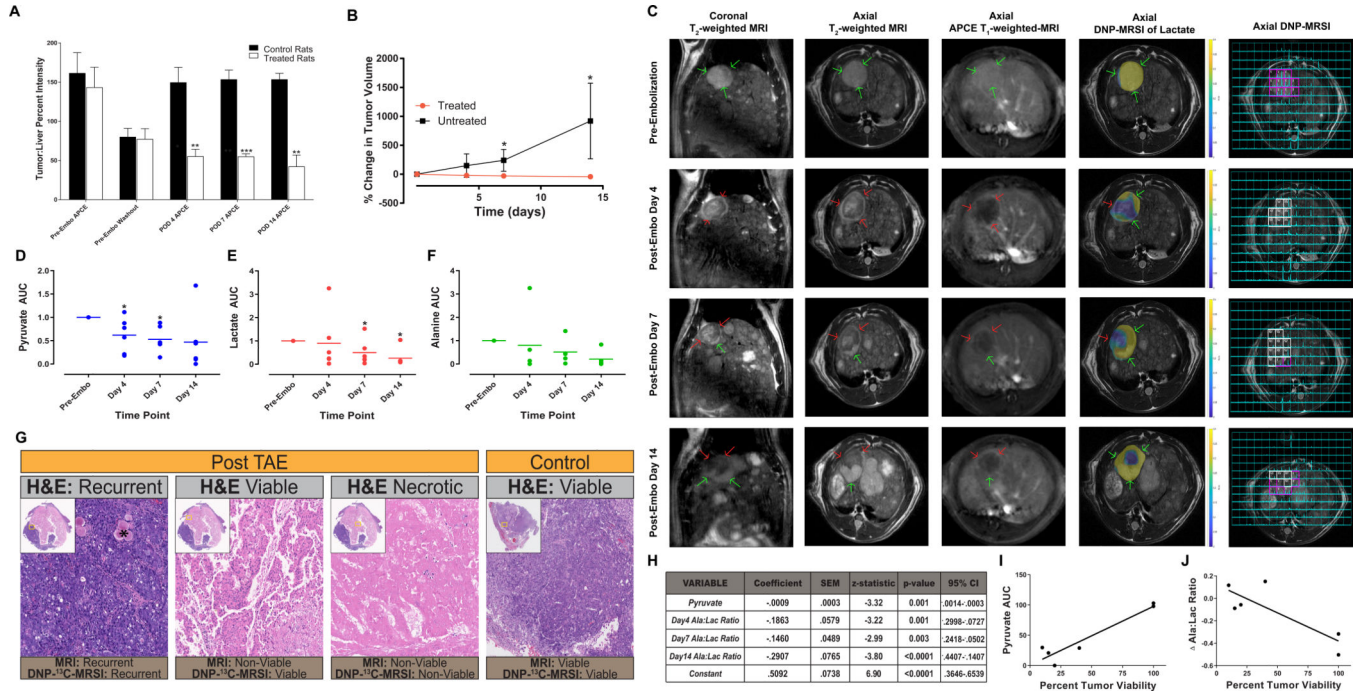

VARIABLE	Coefficient	SEM	z-statistic	p-value	95% CI
Pyruvate	-.0009	.0003	-3.32	0.001	:0014-.0003
Day4 Ala:Lac Ratio	-.1863	.0579	-3.22	0.001	:2998-.0727
Day7 Ala:Lac Ratio	-.1460	.0489	-2.99	0.003	:2418-.0502
Day14 Ala:Lac Ratio	-.2907	.0765	-3.80	<0.0001	.4407-.1407
Constant	.5092	.0738	6.90	<0.0001	.3646-.6539

Figure 5. DNP-MRSI Enables the Detection of Latent HCC Cells Surviving TAE *In Vivo*.

(*A-C*) DEN-induced tumors demonstrate imaging features consistent with the LI-RADS criteria used for image-based diagnosis of HCC in patients including arterial phase contrast enhancement (APCE) and washout on delayed phase imaging relative to uninvolved liver. Images from a representative animal demonstrated T_2-weighted and post-contrast T_1-weighted imaging features consistent with viable HCC (→, V in the final column). Consistent with imaging features observed following a complete response to TAE as assessed using the mRECIST criteria, MRI of TAE-treated HCCs demonstrated (i) a >30% reduction in APCE as compared to uninvolved liver (n=3; p= 0.001 on POD4; p<0.0001 on POD7; p=0.002 on POD14) and (ii) a significant reduction in size (n=6; p=0.023 on POD4; p=0.016 on POD7). (*C*) Images from a representative animal demonstrated that while conventional imaging failed to detect viable tumor cells, DNP-MRSI of hyperpolarized 1-^{13}C-pyruvic acid enabled the detection of persistent metabolism at the tumor periphery corresponding to regions of the tumor that appear non-viable on conventional MRI. In these regions reduced levels of pyruvate (*D*; p=0.046 on POD4, p=0.028 on POD7), lactate (*E*; p=0.046 on POD7; p=0.046 on POD14) and alanine (*F*) were observed. (*C,H*) At each post-TAE time point, tumor regions considered non-viable (→, NV in final column) using conventional contrast-enhanced MRI demonstrated reduced alanine-to-lactate ratios as evidenced by a reduction in the associated coefficient using a generalized model. Interestingly, images from a representative animal demonstrated persistent conversion of pyruvate to lactate on day 4 prior to the development of the development of recurrence on conventional imaging. (*G*) H&E staining of a representative TAE-treated animal 14 days after embolization demonstrated persistent viability in regions of tumor that are considered non-viable based on mRECIST criteria but exhibit persistent metabolism on DNP-MRSI adjacent to regions of necrosis and recurrent HCC. (*I*) In the regions of tumor that appeared non-viable on conventional MRI, a linear regression of the percent tumor viability and intra-

tumoral pyruvate levels at post-TAE day 14 demonstrated a significant positive correlation (R^2=.90, p=.0041). (*J*) Linear regression of percent tumor viability and the change in the intra-tumoral alanine-to-lactate ratio 14 days after TAE demonstrated a significant negative correlation (R^2=.69, p=.04).